Preparation and characterization of layered $LiMn_{1/3}Ni_{1/3}Co_{1/3}O_2$ as a cathode material by an oxalate co-precipitation method

Tae-Hyung Cho, Yuki Shiosaki, Hideyuki Noguchi[*]

Department of Applied Chemistry, Saga University, Honjo 1, Saga 840-8502, Japan

Abstract

The layered $LiMn_{1/3}Ni_{1/3}Co_{1/3}O_2$ cathode materials were synthesized by an oxalate co-precipitation method using different starting materials of LiOH, $LiNO_3$, $[Mn_{1/3}Ni_{1/3}Co_{1/3}]C_2O_4 \cdot 2H_2O$ and $[Mn_{1/3}Ni_{1/3}Co_{1/3}]_3O_4$. The morphology, structural and electrochemical behavior were characterized by means of SEM, X-ray diffraction analysis and electrochemical charge–discharge test. The cathode material synthesized by using $LiNO_3$ and $[Mn_{1/3}Ni_{1/3}Co_{1/3}]C_2O_4 \cdot 2H_2O$ showed higher structural integrity and higher reversible capacity of 178.6 mAh g^{-1} in the voltage range 3.0–4.5 V versus Li with constant current density of 40 mA g^{-1} as well as lower irreversible capacity loss of 12.9% at initial cycle. The rate capability of the cathode was strongly influenced by particle size and specific surface area.
© 2005 Elsevier B.V. All rights reserved.

Keywords: $LiMn_{1/3}Ni_{1/3}Co_{1/3}O_2$; Cathode material; Oxalate co-precipitation; Lithium ion battery

1. Introduction

Recently, a layered transition-metal oxide $LiMn_{1/3}Ni_{1/3}Co_{1/3}O_2$, which is solid solution of $LiCoO_2$ and $LiNi_{0.5}Mn_{0.5}O_2$, is extensively studied as a promising cathode material for lithium ion battery because of its higher reversible capacity, lower cost, milder thermal stability and lower toxicity than commercially used $LiCoO_2$ [1–4]. In this solid solution, the valence states of Ni, Mn and Co are 2+, 4+ and 3+, respectively [3,5]. During charge–discharge process, only divalent Ni and trivalent Co can take part in redox process and tetravalent Mn ion is inactive [3,5]. The electrochemically inactive tetravalent Mn is believed to support the host structure during redox process and contribute stable cycling performance.

In our previous study, we reported that electrochemical performance of the $LiMn_{1/3}Ni_{1/3}Co_{1/3}O_2$ solid solution is strongly affected by synthesis condition for the sake of difference in homogeneity [6]. Thus, we believe that the control of homogeneity and integrity of the host structure are most important factors to obtain better electrochemical properties such as high reversible capacity and stable cycling performance.

However, preparation of the $LiMn_{1/3}Ni_{1/3}Co_{1/3}O_2$ solid solution with excellent electrochemical performance is quite difficult. A hydroxide co-precipitation method has been used as a major preparation technique to get homogeneous solid solution [1–4,7–9]. Obviously, the hydroxide co-precipitation is one of the powerful synthesis methods. During the precipitation period, however, precipitated transition-metal hydroxide oxidizes in the aqueous solution. For example, $Mn(OH)_2$ oxidizes gradually to MnOOH (Mn^{3+}) or MnO_2 (Mn^{4+}) upon precipitation conditions which can decrease the homogeneity of final product. Therefore, the control of valence state of Mn in aqueous solution is a critical point to obtain homogeneous solid solution. In our previous work [10,11], we applied carbonate co-precipitation method to prepare homogeneous precursor by fixing the valence of Mn during precipitation process. Consequently, we had successfully synthesized $LiMn_{1/3}Ni_{1/3}Co_{1/3}O_2$ cathode material with excellent electrochemical performance.

Here, therefore, we selected an oxalate co-precipitation method for synthesis $LiMn_{1/3}Ni_{1/3}Co_{1/3}O_2$ solid solution because the valence state of Mn in oxalate form can be stable as +2 in an aqueous solution. This implies that the homogeneous solid solution containing Mn could be readily prepared using oxalate co-precipitation method. In this study, we reported the structural integrity, morphology and electrochemical performances of the $LiMn_{1/3}Ni_{1/3}Co_{1/3}O_2$ cathode material prepared

---
[*] Corresponding author. Tel.: +81 952 28 8674; fax: +81 952 28 8591.
E-mail address: noguchih@cc.saga-u.ac.jp (H. Noguchi).

by oxalate co-precipitation method. And we also reported the effects of the starting materials on the electrochemical properties of the $LiMn_{1/3}Ni_{1/3}Co_{1/3}O_2$ cathode material.

2. Experimental

LiOH, $LiNO_3$, $Mn(NO_3)_2\cdot6H_2O$, $Ni(NO_3)_2\cdot6H_2O$, $Co(NO_3)_2\cdot6H_2O$ and $(NH_3)_2C_2O_4$ were used as starting materials. To form a transition-metal oxalate $[Mn_{1/3}Ni_{1/3}Co_{1/3}]C_2O_4$, we prepared two aqueous solutions, transition-metal nitrate and a 0.15 M ammonium oxalate. A white $[Mn_{1/3}Ni_{1/3}Co_{1/3}]C_2O_4$ sediment was obtained by dropping these solutions into hot reaction bath (60 °C) at the same time in an inert atmosphere. During precipitation, the pH of the reaction bath was adjusted by adding of NH_4OH to 8.5. After precipitation, the sediment was filtered with distilled water several times then was dried at room temperature.

The thermal behavior of obtained metal oxalate was confirmed by TG–DTA analysis with a scan rate of 10 °C min^{-1} in air atmosphere.

In order to investigate the effect of starting material on the structural and electrochemical performance of synthesized cathode material, we used two types of transition-metal precursors, an oxalate or an oxide. A transition-metal oxide was prepared by the decomposition of oxalate sediment at 500 °C for 5 h in air. The decomposition from transition-metal oxalate into transition-metal oxide was confirmed by thermogravimetry analysis and X-ray diffraction methods.

$LiMn_{1/3}Ni_{1/3}Co_{1/3}O_2$ solid solutions were synthesized by the calcination of a stoichiometric amount of LiOH or $LiNO_3$ and transition-metal oxalate or transition-metal oxide at 1000 °C for 20 h in air. Before calcination, the exact amounts of the transition-metal ions in transition-metal oxalate or transition-metal oxide were determined by EDTA titration technique [12].

X-ray diffraction measurements for the precursor and the synthesized $LiMn_{1/3}Ni_{1/3}Co_{1/3}O_2$ materials were carried out using a Cu Kα radiation of Rigaku Rint 1000 diffractometer in the scanning range (2θ) of 10–80°. The specific surface areas of the synthesized materials were measured using a Micromeritics Gemini 2375 (USA) by the BET method. Scanning electron microscopy (SEM: JSM-5300E, JEOL, Japan) was carried out to observe the morphologies of the synthesized materials.

The electrochemical characterizations were carried out using the CR-2032-type coin cell. A cathode was prepared by pressing active material film, which is consist of 20 mg active material and 12 mg conducting binder (Teflonized acetylene black), on the stainless steel mesh. The coin type cell was composed of the cathode, the lithium foil as an anode and 1 M $LiPF_6$-EC/DMC (1:2 in volume) as an electrolyte. The electrochemical cycling tests were performed at room temperature.

3. Results and discussions

3.1. Characterization of co-precipitated compound

The metal oxalate can be established two different crystal-hydrated types depending on the precipitation conditions;
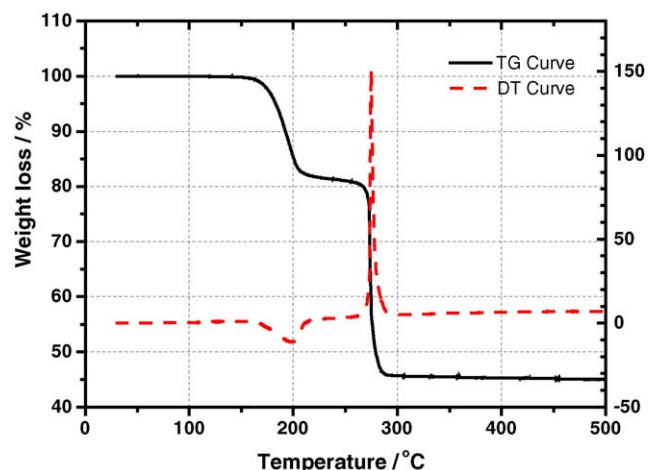

Fig. 1. Thermogravimetric analysis profile for the $[Mn_{1/3}Ni_{1/3}Co_{1/3}]C_2O_4\cdot2H_2O$.

$MeC_2O_4\cdot2H_2O$ and $MeC_2O_4\cdot3H_2O$ (Me = metal ion) [13,14]. The former is a white colored metal oxalate dihydrate, monoclinic structure and the latter is a pink colored metal oxalate trihydrate, orthorhombic structure. As described in Section 2, we obtained a white sediment in the conditions of 60 °C, an inert atmosphere and pH 8.5. Based on the color of the sediment, we believe that the sediment prepared in this study is $[Mn_{1/3}Ni_{1/3}Co_{1/3}]C_2O_4\cdot2H_2O$ with monoclinic structure. The suggested chemical composition and thermal behavior of obtained metal oxalate were confirmed and discussed below.

Fig. 1 shows the TG–DTA curve for the transition-metal oxalate. The profile had two steps of weight loss. The first step from 160 to 220 °C showed ca. 19.5 wt.% weight loss with small broad endothermic peak in DTA curve that would be related with dehydration of metal oxalate. In suggesting chemical formula of metal oxalates by earlier literatures [13,14], $MeC_2O_4\cdot2H_2O$ and $MeC_2O_4\cdot3H_2O$ can be dehydrated by thermal treatment. Hence, 19.8 and 27.1 wt.% of weight losses by losing of crystal water are expected for the $MeC_2O_4\cdot2H_2O$ and $MeC_2O_4\cdot3H_2O$, respectively. The 19.5 wt.% of weight loss in the first step determined by TG experiment agrees well with the value of 19.8 wt.% that is calculated from the dehydration of $MeC_2O_4\cdot2H_2O$. Therefore, the chemical formula of prepared metal oxalate can be represented as $[Mn_{1/3}Ni_{1/3}Co_{1/3}]C_2O_4\cdot2H_2O$ as expected. Total metal ion content determined by the EDTA analysis [12] also agrees with this composition. Consequently, the possible dehydration reaction in the first weight loss could be described in Eq. (1):

$$[Mn_{1/3}Ni_{1/3}Co_{1/3}]C_2O_4\cdot2H_2O$$
$$\rightarrow [Mn_{1/3}Ni_{1/3}Co_{1/3}]C_2O_4 + 2H_2O \uparrow \qquad (1)$$
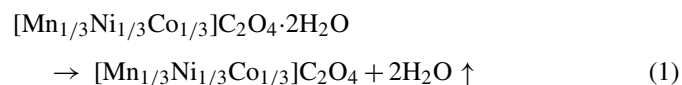
After dehydration reaction, the anhydrous $[Mn_{1/3}Ni_{1/3}Co_{1/3}]C_2O_4$ can be decomposed into both metal oxide and gases such as carbon mono- and di-oxide by further thermal treatment in air. The weight loss in the second step with large sharp exothermic DTA curve was observed around 270 °C. However, there are no changes in both TG and DTA curves up to 500 °C. This second weight loss with exothermic reaction is probably

the decomposition of anhydrous $[Mn_{1/3}Ni_{1/3}Co_{1/3}]C_2O_4$. The possible decomposition reaction in air is suggested in Eq. (2):

$$3[Mn_{1/3}Ni_{1/3}Co_{1/3}]C_2O_4 + 2O_2$$
$$\rightarrow [Mn_{1/3}Ni_{1/3}Co_{1/3}]_3O_4 + 6CO_2\uparrow \qquad (2)$$
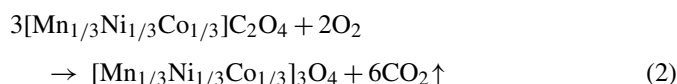
In the equation, 3 mol anhydrous $[Mn_{1/3}Ni_{1/3}Co_{1/3}]C_2O_4$ can be transform into 1 mol $[Mn_{1/3}Ni_{1/3}Co_{1/3}]_3O_4$ with 6 mol of CO_2 gases with releasing some energy. The theoretical value of weight loss in this reaction is 35.3 wt.%. This value is well coincident with the observed value 35.2 wt.%. We carried out XRD analysis in order to investigate structural change during the thermal decomposition process. Fig. 2 shows X-ray diffraction patterns of oxalate precursor and thermally decomposed oxide compound. The diffraction pattern of oxalate (Fig. 2a) is well agreed with monoclinic α-$FeC_2O_4 \cdot 2H_2O$ (JCPDS No. 22-0355). A Me_3O_4 (Me = metal) is typical formula of spinel compound. The sample prepared by heating at 500 °C for 5 h in air atmosphere shows a typical XRD profile of spinel structure (space group: 227, $Fd3m$) as seen in Fig. 2b. Based on the TG–DTA and XRD results, it is clear that we have prepared α-$[Mn_{1/3}Ni_{1/3}Co_{1/3}]C_2O_4 \cdot 2H_2O$ with monoclinic structure and this metal oxalate dihydrate transformed into $[Mn_{1/3}Ni_{1/3}Co_{1/3}]_3O_4$ through dehydration and decomposition reactions by thermal treatment in air.
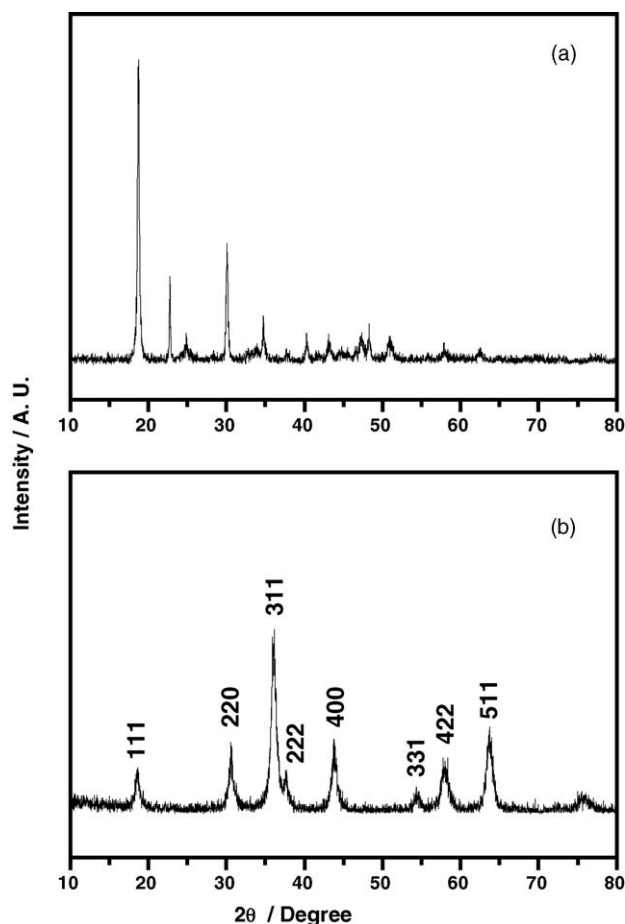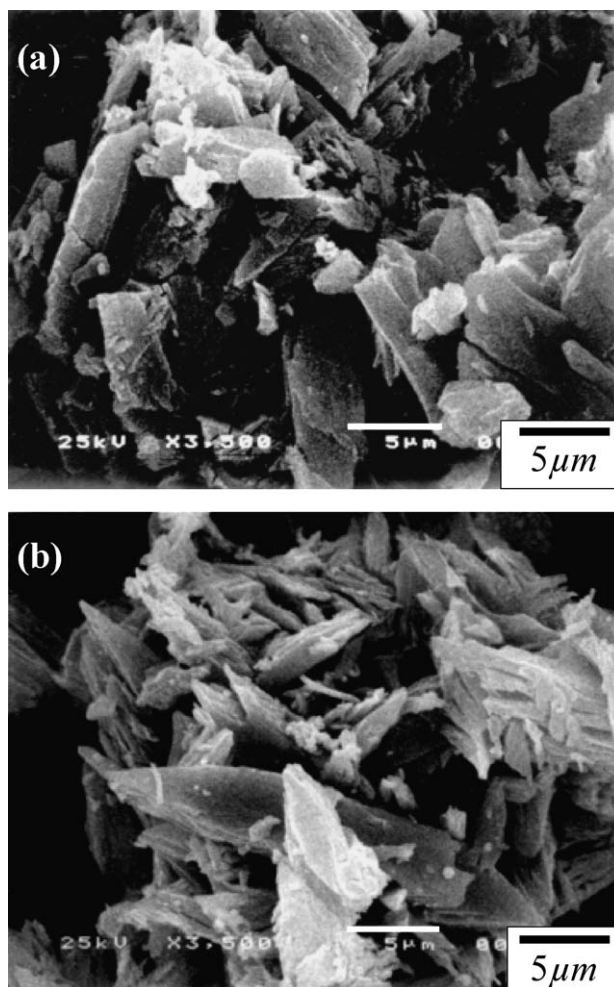

Fig. 3. SEM photographs of: (a) oxalate precursor and (b) thermally decomposed compound at 500 °C for 5 h.

Fig. 3a and b shows SEM photographs of an oxalate precursor and thermally decomposed spinel oxide, respectively. As shown in Fig. 3, the large oxalate particles (Fig. 3a) broke into small narrow particles (Fig. 3b) during the thermal decomposition process, due probably to vigorous evaporation of CO_2 gases.

3.2. Characterization of cathode compounds

In order to observe the morphologies of the synthesized cathode materials, SEM observation was carried out. The SEM images of four samples are shown in Fig. 4. Where the specific surface areas determined by BET technique are also described. The four samples had clearly different morphology and specific surface area. The sample A, which synthesized using oxalate precursor and lithium hydroxide, showed irregular particle shape and flat surface in addition to the largest particle size of 5–10 μm. On the other hand, sample D synthesized from oxide precursor and lithium nitrate had the smallest particle size (less than 1 μm) among them. The specific surface areas of samples A, B, C and D were 0.27, 0.56, 0.80 and 1.02 m^2 g^{-1}, respectively. Consequently, SEM observation and BET measurement revealed that

Fig. 2. X-ray diffraction patterns of: (a) $[Mn_{1/3}Ni_{1/3}Co_{1/3}]C_2O_4 \cdot 2H_2O$ and (b) $[Mn_{1/3}Ni_{1/3}Co_{1/3}]_3O_4$.
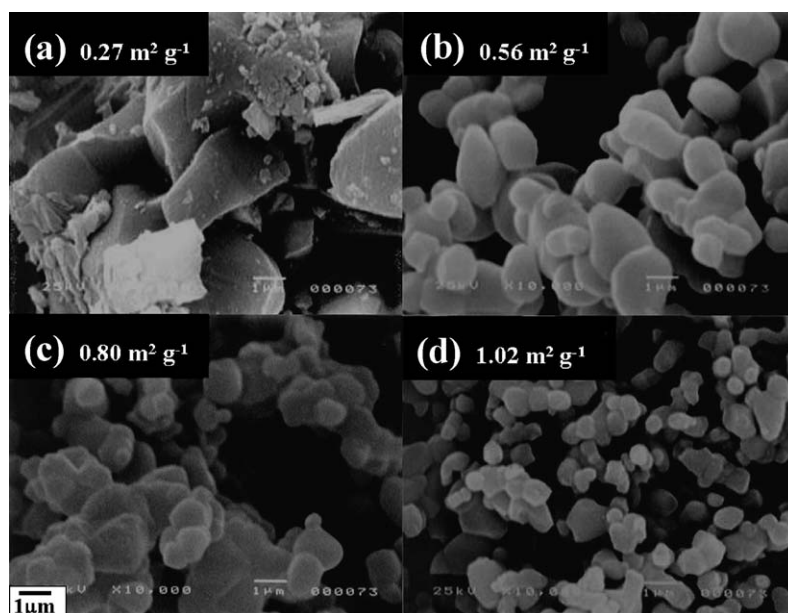
Fig. 4. SEM photographs and specific surface areas for the (a) sample A, (b) sample B, (c) sample C and (d) sample D.
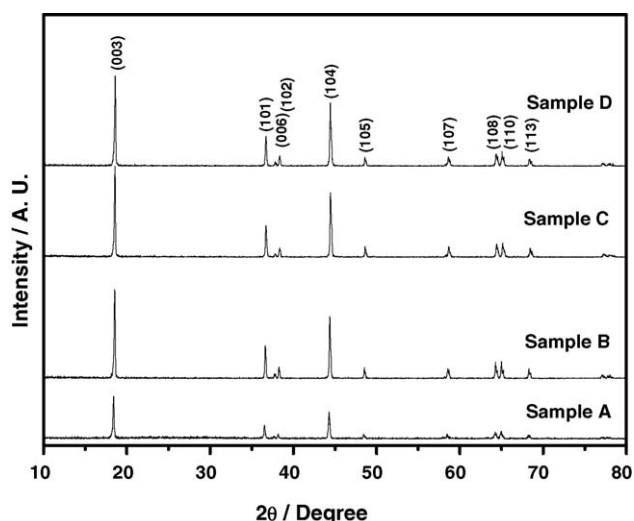

Fig. 5. X-ray diffraction patterns for the synthesized $LiMn_{1/3}Ni_{1/3}Co_{1/3}O_2$ cathode materials.

the contribution of lithium nitrate and transition-metal oxide lead smaller particle size and large specific surface area than that of the lithium hydroxide and the metal oxalate.

Fig. 5 shows the results of XRD studies for the synthesized $LiMn_{1/3}Ni_{1/3}Co_{1/3}O_2$ materials using various lithium sources with metal oxalate or metal oxide at 1000 °C. The XRD patterns of all materials could be indexed based on the α-NaFeO$_2$ structure (space group: 166, $R\bar{3}m$). We could not observe any impurity phases in the measured range and all samples showed clear peak split of (006, 102) and (108, 110), which is an indicator of hexagonal ordering [15,16]. The lattice parameters of the synthesized cathode materials were calculated by least square method using 10-diffraction lines. The determined parameters are summarized together with starting materials in Table 1. The determined lattice parameters were somewhat different for the samples. The sample C showed the smallest lattice parameter a and c, which are very close with reported values [1,3,11]. On the other hand, the sample A showed bigger lattice parameters a and c than others. Samples B and D showed intermediate values of lattice parameters between samples C and A. This difference in lattice parameter indicates that the samples were synthesized with different structural integrity because lattice parameters closely related with atomic distribution (e.g. cation mixing) in hexagonal oxide cathode material. The trend of degree of cation mixing in the samples have been traced by intensity ratio, $R = [I_{(102)} + I_{(006)}]/I_{(101)}$, which was suggested by Reimers et al. [17] to deduce degree of cation mixing in Ni-based layered cathode material. Here, the lower R value indicates lower cation mixing. From the calculation of intensity ratio, it was found that the sample C prepared using LiNO$_3$ and metal oxalate shows the highest structural integrity, i.e. lower cation mixing, whereas the sample A prepared using LiOH and metal oxalate shows the lowest one. Therefore, it could be expected that the sample C prepared using LiNO$_3$

Table 1
Summary of starting materials and structural parameters of synthesized $LiMn_{1/3}Ni_{1/3}Co_{1/3}O_2$ cathode materials

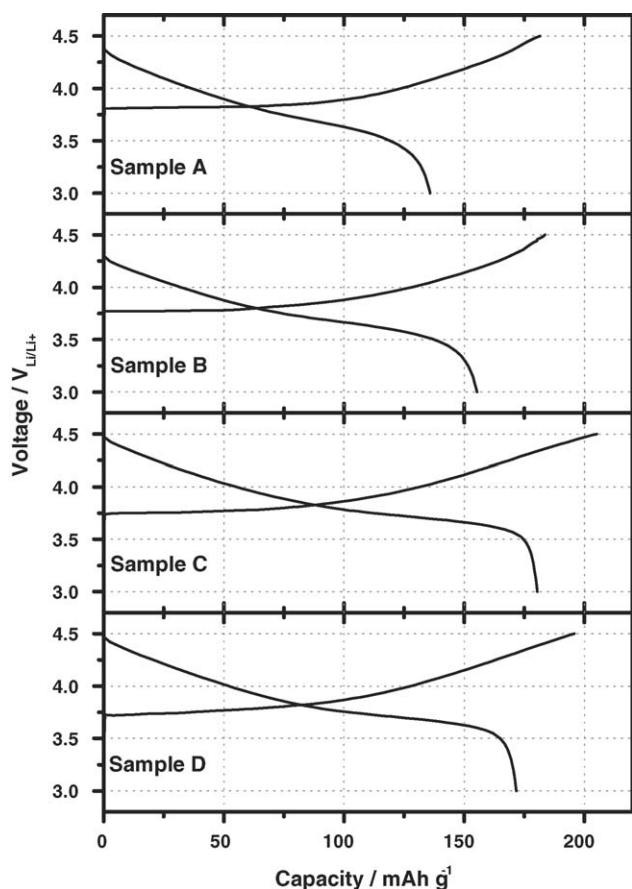| Sample	Starting materials		a (Å)	c (Å)	c/a	Vol. (Å^3)	$I_{(006+102)}/I_{(101)}$
A	$MC_2O_4 \cdot 2H_2O$	LiOH	2.869	14.299	4.983	101.99	0.60
B	M_3O_4	LiOH	2.868	14.271	4.975	101.65	0.50
C	$MC_2O_4 \cdot 2H_2O$	LiNO$_3$	2.863	14.244	4.976	101.16	0.42
D	M_3O_4	LiNO$_3$	2.864	14.254	4.977	101.32	0.49

Fig. 6. Initial charge and discharge curves for the synthesized LiMn$_{1/3}$Ni$_{1/3}$Co$_{1/3}$O$_2$ cathode materials.

and metal oxalate can deliver better electrochemical performance than other samples due to a better structural integrity than others.

3.3. Electrochemical characteristics

The electrochemical charge–discharge experiments for the four LiMn$_{1/3}$Ni$_{1/3}$Co$_{1/3}$O$_2$ samples were carried out at room temperature in the voltage range between 3.0 and 4.5 V versus Li. A constant current density of 40 mA g^{-1} (0.4 mA cm^{-2}) was applied to working electrode. Initial charge–discharge curves and cycle stability for the cells are presented in Figs. 6 and 7, respectively. The highest initial discharge capacity of 178.6 mAh g^{-1} and the lowest irreversible capacity of 12.9% were obtained from sample C. It is superior capacity than a capacity (155 mAh g^{-1}) observed from a cathode prepared by solid-state reaction method [6]. Moreover, it is comparable to capacities obtained from other solution methods [3,11,18]. The lowest discharge capacity of 133.2 mAh g^{-1} and the highest irreversible capacity of 26.6% were obtained by sample A. The samples B and D delivered 152.4 and 170.0 mAh g^{-1} as initial discharge capacity and showed irreversible capacity of 15.6 and 13.2%, respectively. The obtained electrochemical performances of cathodes revealed that there is a close relationship between structural integrity and electrochemical performance. Therefore, it could be concluded that electrochemical proper-
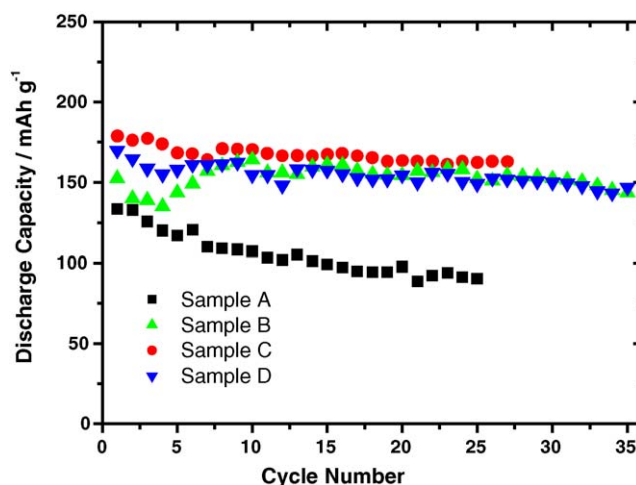
ties of the cathode material depend strongly on the structural integrity.

Fig. 7 shows cycle stability of the four samples. As shown in Fig. 7, cycle stability also depended strongly on the structural integrity. The sample C, which has the highest structural integrity, showed highest retained discharge capacity of 162.3 mAh g^{-1} after 25 cycles. On the other hand, sample A, which has the lowest structural integrity, showed the lowest retained discharge capacity of 86 mAh g^{-1}. In the case of the samples B and D, which have similar structural integrity, showed almost same cycling performance after 10th cycle, in spite of difference in initial capacity.

Fig. 7. Discharge capacities as a function of cycle number for the synthesized LiMn$_{1/3}$Ni$_{1/3}$Co$_{1/3}$O$_2$ cathode materials in the voltage range 3.0–4.5 V.
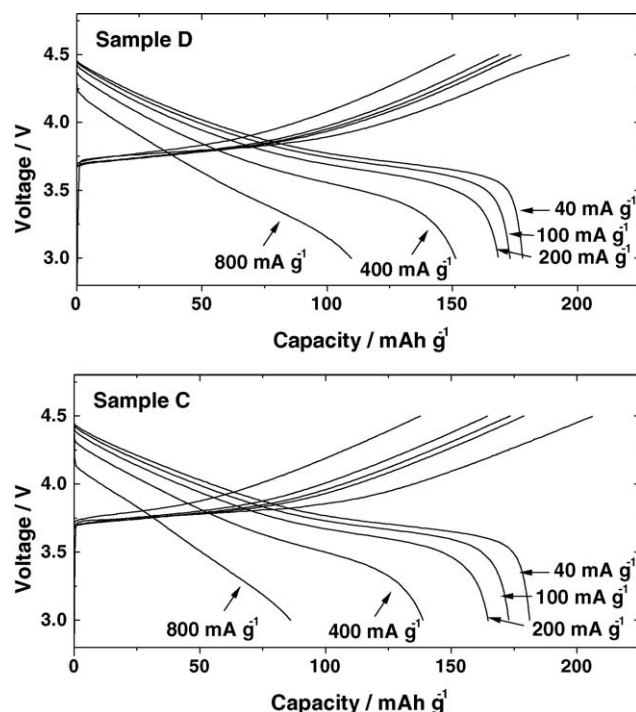

Fig. 8. Rate capability tests for the samples D and C in the voltage range 3.0–4.5 V.

In order to investigate the rate capability of the samples C and D, we applied constant current of $40\,\mathrm{mA\,g^{-1}}$ (0.22 C) for charging and various current densities of 40, 100, 200, 400 and $800\,\mathrm{mA\,g^{-1}}$ for the discharge in the voltage range of 3.0–4.5 V versus Li. The results are presented in Fig. 8. The C rates were calculated using $180\,\mathrm{mAh\,g^{-1}}$ as a theoretical capacity. The sample C delivered slightly higher initial discharge capacity of $181.2\,\mathrm{mAh\,g^{-1}}$ than that of the sample D ($178.1\,\mathrm{mAh\,g^{-1}}$). However, the sample D showed higher capacity retention ratio than that of the sample C with increasing current density thereby when the $800\,\mathrm{mA\,g^{-1}}$ (4.44 C) was applied to the cathodes, the retained discharge capacities of the samples C and D were 86.2 and $109.8\,\mathrm{mAh\,g^{-1}}$, respectively. The better rate capability of the sample D than that of sample C is due probably to small particle size and large specific surface.

4. Conclusion

The layered $LiMn_{1/3}Ni_{1/3}Co_{1/3}O_2$ cathode materials were successfully synthesized by using homogeneous Mn, Ni and Co mixture, which was prepared by the oxalate co-precipitation, LiOH and $LiNO_3$ as starting materials. The XRD experiment and SEM observation revealed that structural integrity and morphology of the cathode materials synthesized using oxalate compound strongly depend on the lithium sources. Lithium nitrate delivered better structural integrity and homogeneous particle distribution than lithium hydroxide. The sample C delivered higher reversible capacity of $178.6\,\mathrm{mAh\,g^{-1}}$ as well as lower irreversible capacity loss of 12.9% with help of higher structural integrity. From the rate capability test, small particle sized powder with large specific surface area can show excellent rate capability.

References

[1] T. Ohzuku, Y. Makimura, Chem. Lett. (2001) 642.
[2] N. Yabuuchi, T. Ohzuku, J. Power Sources 119–121 (2003) 171.
[3] K.M. Shaju, G.V. Subba Rao, B.V.R. Chowdari, Electrochim. Acta 48 (2002) 145.
[4] I. Belharouak, Y.-K. Sun, J. Liu, K. Amine, J. Power Sources 123 (2003) 247.
[5] W.-S. Yoon, C.P. Grey, M. Balasubramanian, X.-Q. Yang, D.A. Fischer, J. McBreen, Electrochem. Solid-State Lett. 7 (2004) A53.
[6] D. Li, T. Muta, L. Zhang, M. Yoshio, H. Noguchi, J. Power Sources 132 (2004) 150.
[7] Z. Lu, D.D. MacNeil, J.R. Dahn, Electrochem. Solid-State Lett. 4 (2001) A200.
[8] D.D. MacNeil, Z. Lu, J.R. Dahn, J. Electrochem. Soc. 149 (2002) A1332.
[9] M.-H. Lee, Y.-J. Kang, S.-T. Myung, Y.-K. Sun, Electrochim. Acta 50 (2004) 939.
[10] T.H. Cho, S.M. Park, M. Yoshio, Chem. Lett. 33 (2004) 704.
[11] T.H. Cho, S.M. Park, M. Yoshio, T. Hirai, Y. Hideshima, J. Power Sources 142 (2005) 306.
[12] Y.S. Lee, Y.K. Sun, K. Adachi, M. Yoshio, Electrochim. Acta 48 (2003) 1031.
[13] R. Deyrieux, C. Berro, A. Peneloux, Bull. Soc. Chim. Fr. 1 (1973) 25.
[14] A. Juizing, H.A.M. van Hal, W. Kwestroo, C. Lahgereis, P.C. van Loosdregt, Mater. Res. Bull. 12 (1977) 605.
[15] J.R. Dahn, U. von Sacken, A.V. Chadwick, Solid State Ionics 44 (1990) 87.
[16] T. Ohzuku, A. Ueda, M. Nagayama, J. Electrochem. Soc. 140 (1993) 1862.
[17] J.N. Reimers, J.R. Dahn, J.E. Greedan, C.V. Stager, G. Liu, I. Davidson, U. von Sacken, J. Solid State Chem. 102 (1993) 542.
[18] S.H. Park, C.S. Yoon, S.G. Kang, H.-S. Kim, S.-I. Moon, Y.-K. Sun, Electrochim. Acta 49 (2004) 557.